A Mach-Zehnder Interferometer Based on Balanced Broadband Directional Couplers

Jingwei Liu, *jingwei_liu@hotmail.com*

***Abstract*—This report presents the design, simulation, and experimental result of a silicon-on-insulator (SOI) based, strip waveguide, Mach-Zehnder interferometer based on two balanced broadband directional 50/50 couplers. Different path length difference ΔL's are used to study ΔL impact on free spectral range (FSR), and to show the typical interferometer constructive-destructive patterns. Theoretical analysis, Lumerical simulation and experimental result are cross checked. The experimental results match the Lumerical simulations to better than 2% with path length difference down to 50μm. At 400μm path length difference, both the experimental FSR and peak wavelength fall within the Monte Carlo simulation range. The group index extracted from the experimental result falls within the span defined by the four corner conditions. Local effective device width/height may be extracted from the group index matching between experimental result and eigenmode simulation. A 0.01nm FSR difference (1.425 vs. 1.435nm), a 0.0034 group index difference (4.1857 vs. 4.1823), a 2nm width difference (501 vs. 503nm), and a 0.5nm height difference (221 vs. 220.5nm), are observed when two MZIs with 400μm path length difference are placed around 7mm away. Due to the manufacturing variation, the structural feature width/height is pretty local, and may be good for local usage only. The local width/height may not be used for other devices nor be used as a universal value for all devices across the wafer. Two designed 90:10 splitters, which are placed around 7mm away, become one 69:31 splitter and one 77:23 splitter due to the conceptual introduction of an "effective" extra path length difference of 61.39nm and 42.82nm, respectively, induced by the manufacturing variation. Similarly, the designed balanced MZI becomes a 96:4 splitter with an introduced "effective" extra path length difference of 41.39nm. The manufacturing variation induced "effective" extra path length difference may vary from device to device, and from location to location.**

***Index Terms*—silicon photonics, silicon-on-insulator, strip, Mach-Zehnder, broadband directional coupler, gain, balanced, splitter, free spectral range, corner analysis, simulation, Ebeam.**

I. INTRODUCTION

IN the past two decades, photonic integrated circuits (PIC), in the broader context, and silicon photonics (Si-Phy), in a more specific scope, have significantly contributed to the fast evolution of the optical communication industry and artificial intelligence (AI) industry [1] [2]. With the usage of the mature and well-developed complementary metal oxide semiconductor (CMOS) fabrication technology, compared to non-silicon photonics devices, silicon photonics devices show advantages of better performance, higher speed, reduced loss, reduced power consumption, better manufacturing uniformity, and CMOS compatibility. These advantages make silicon photonics the nature choice for optical communication and AI.

The Mach-Zehnder interferometer (MZI) is an important element for lots of optical devices such as optical modulators, switches, wavelength division multiplexer (WDM), and even new-generation reconfigurable optical add-drop multiplexer [3], [4].

This work is devoted to explaining the design, simulation, and characterization of a silicon-on-insulator (SOI) based, strip waveguide, MZI devices based on two balanced broadband directional 50/50 coupler/splitters.

II. DESIGN

In silicon photonics, the research and developmental work is mainly focused on a subwavelength geometry, in which a silicon waveguide core is formed over a silicon substrate interleaved by a 2–3 μm-thick silica buried oxide (BOX) layer – so-called "silicon on insulator (SOI)" configuration. The most used thickness of the silicon core is 220 nm. The large refractive index contrast (for example, 3.48 vs. 1.44, $\Delta n > 2$ at 1550 nm) between the silicon core and the surrounding oxide ensures strong confinement of the light guided in a strip- (a) or a rib- (b) shape waveguide as shown in Fig. 1 [1]. Typically, the waveguides are fabricated from a vendor provided SOI wafer, consisting of four layers: silicon substrate, BOX, silicon waveguide, and cladding oxide. The SOI wafer, including BOX and silicon core, is fabricated by SOI wafer venders. While silicon etch and cladding oxide is fabricated from users' place, typically, a non-SOI-wafer vender fab/lab, for example, a university or institute cleanroom/lab. There is a chance the two oxides (BOX and cladding oxide) may have slightly different material property and reflection index. We ignore this slight difference and use the standard oxide in PDK library to represent them in simulation. Waveguides are used for routing purposes, like wires in electrical circuits. Compared to the rib waveguides, the strip waveguides are more friendly for beginner researchers for the less fabrication steps (1 step silicon etch vs. 2 steps for rib waveguides), smaller bending radius, stronger confinement, while at the sacrifice of higher loss due to sidewall roughness impact [5].

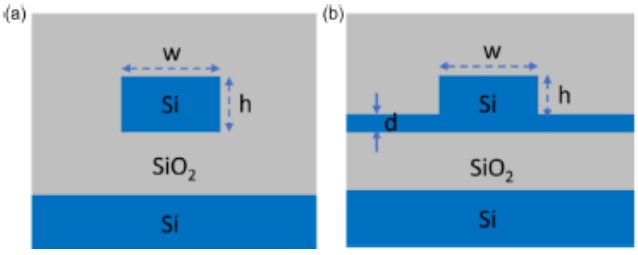

Fig. 1. Cross section of strip (a) and rib (b) waveguides.

This manuscript was submitted on 07/05/2025

Strip waveguides with 220nm height (h) – which is usually the thickness of silicon core in SOI wafers, 500nm width (w), wavelength at 1550nm with TE mode, are used for this study.

The Mach-Zehnder interferometer (MZI) is an important element for lots of optical devices. MZI's can be built from multiple different choices. For example, an MZI can be built from two ideal 2x2 splitters and two waveguides with path length difference ΔL as shown in Fig. 2.

This ideal MZI has a transfer function of

$$\frac{I_o}{I_i} = \frac{1}{2}[1 + \cos\beta\Delta L] \quad (1)$$

where I_i is the input light intensity, I_o is the output intensity at the bottom port (through bar), ΔL is the path length difference between the two waveguides, β is the waveguide propagation constant and is defined by

$$\beta = \frac{2\pi n}{\lambda} \quad (2)$$

where n is the waveguide effective index (which is typically wavelength dependent), and λ is the wavelength, 1550nm in this study.

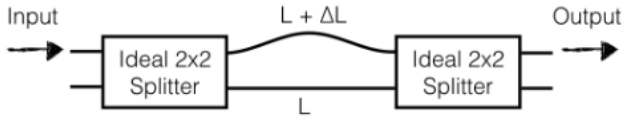

Fig. 2. Conceptual drawing of one MZI configuration.

For the output at the top port (cross port), the ideal transfer function is

$$\frac{I_o}{I_i} = \frac{1}{2}[1 - \cos\beta\Delta L] \quad (3)$$

The sum of Eq. 1 (through bar) and Eq. 3 (cross port) is always 1. In ideal conditions, all light intensity is transferred through either bottom port (through bar), or top port (cross port), without any loss. Also, the peak (maximum value) of Eq. 1 is the valley (minimum value) of Eq. 3, and vice versa. We will expect to see the peak/valley reversion at the gain vs. wavelength plots.

The Eq. 1 (through bar) transfer function is 1, in other words, I_o is with the same amplitude as I_i – constructive, when

$$\beta\Delta L = 2m\pi \quad (4)$$

; while is 0, in other words, I_o is zero – destructive, when

$$\beta\Delta L = (2m+1)\pi \quad (5)$$

where m is any integer.

At large ΔL, say, 400μm, within a reasonable wavelength range, say, 100nm, we may see multiple (λ, m) combinations meeting constructive (Eq. 1) and destructive (Eq. 3) conditions for both through bar and cross port, thus multiple peaks and valleys in the gain vs. wavelength plots.

At small ΔL, say, on the order of 10's of nm, the input light intensity will be split between through bar and cross port as shown in Eq. 1 and Eq. 3, and the MZI will work as a splitter.

Typically, a de-embedding structure composed of two fiber grating couplers (GCs) connected by a waveguide, is used to calibrate the measurement system insertion loss. In this study, two de-embedding structures with waveguide length of 250μm and 500μm, are used to calibrate the measurement system insertion loss, and to measure the silicon waveguide intrinsic loss. Ideally, due to the waveguide length difference, the loss difference between the longer and shorter waveguide is from the intrinsic loss of the 250μm longer waveguide.

In waveguide compact mode, one can perform a curve fit of the effective index (n_{eff}) versus wavelength (λ), where n_1, n_2, and n_3 are called waveguide parameters.

$$n_{\text{eff}}(\lambda) = n_1 + n_2(\lambda - \lambda_0) + n_3(\lambda - \lambda_0)^2 \quad (6)$$

III. Simulation

Strip waveguides with 220nm height (h), 500nm width (w), 1550nm wavelength with TE mode, and two balanced broadband directional 50/50 coupler/splitters (bdc, similar function as the Fig. 2 2x2 ideal splitter) are used for this study.

Fig. 3 shows the Lumerical simulation configuration. The light signal from the output of the optical network analyzer ONA_1 is fed as input into the top port (opt_1) of the ebeam_bdc_te1550_1 (bdc_1). On the output side, the opt_1 (through bar) and opt_2 (cross port) of ebeam_bdc_te1550_2 (bdc_2) is fed into input 1 and 2 of ONA_1, respectively. The Opt_2 of bdc_1 is fed into input 3 of ONA_1 to track any reflected-back signal. In ideal coupler/splitter calculation, we assume that the phases are equal at the two outputs of each coupler/splitter. In a real coupler/splitter, this is not the case. In this study, "point symmetric" balanced configuration [6] is used to create the MZI such that the phase differences are cancelled out for the two bdc coupler/splitters. In this study, the 2nd bdc (bdc_2) is flipped both vertically and horizontally relative to the 1st bdc (bdc_1).

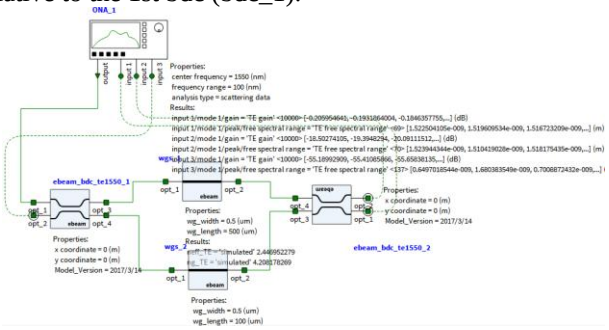

Fig. 3. Conceptual simulation of two balanced bdc MZI.

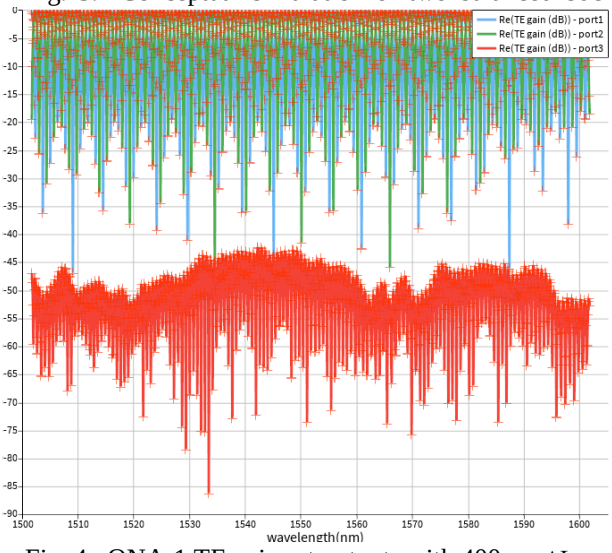

Fig. 4. ONA-1 TE gains at outputs with 400μm ΔL.

At path length difference (ΔL) of 400μm, the three ONA-1 inputs are plotted in Fig. 4, with zoomed-in shown in Fig. 5. The classical MZI construction/destruction patterns are clearly shown at input 1 and input 2 of ONA-1. The expected peak-valley reversion is clearly seen on port 1 vs. port 2 in Fig. 5. The "reflected-back" signal from the input 3 of ONA-1 (opt_2 of bdc_1) is less than -40dB and is usually negligible.

The free spectral range (FSR) can be extracted from the transfer function plots of the "pure" ideal Lumerical Simulation (without actual layout, named as "Lumerical Simulated FSR" in Table 1), of the Klayout layout based Lumerical Simulation (named as "Klayout Simulated FSR" in Table 1), or of the experimental result of the fabricated devices (named as "Exp. FSR" in Table 1).

The relation between free spectral range (FSR) and path length difference ΔL, wavelength λ, and group index n_g, is expressed in Eq. 7.

$$\mathrm{FSR} = \Delta\lambda = \frac{\lambda^2}{\Delta L\left(n - \lambda\frac{dn}{d\lambda}\right)} = \frac{\lambda^2}{\Delta L n_g} \quad (7)$$

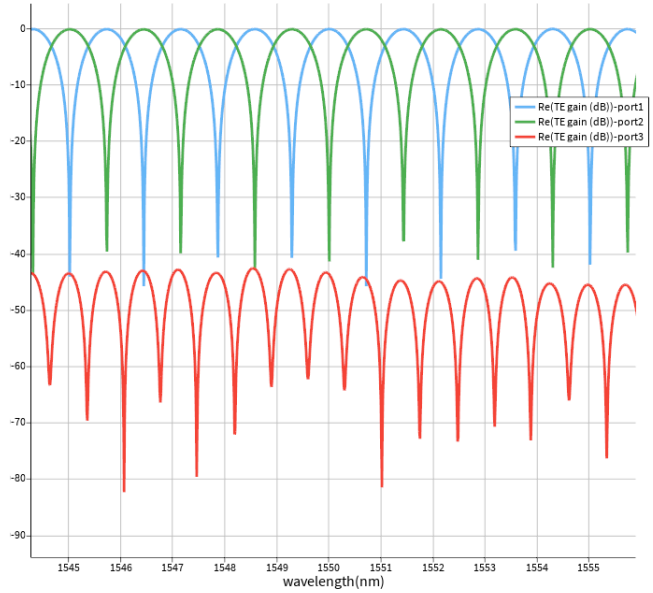

Fig. 5. Zoomed-in around wavelength 1550nm from Fig. 4.

Group index (n_g) is material and waveguide cross sectional geometry, i.e., width and height, dependent but not waveguide length dependent. At a fixed λ, say, 1550nm, group index (n_g) is constant and does not change with ΔL. From Eq. 7, FSR should be reversely appropriate to ΔL. The longer the ΔL is, the smaller the FSR is. Five different ΔL's, 400μm, 200μm, 100μm, 50μm, and 25μm, are used to simulate the ΔL impact on FSR. The FSR is extracted from the simulated gain peak closest to, but not exactly at, 1550nm. As shown in Table 1, the multiplication of (ΔL x FSR for Lumerical simulation) is pretty stable at 567-571, with only about 1% variation. The small variation may be due to the slight shift of the nearest gain peak from 1550nm.

Another usage of an imbalanced MZI is a splitter, i.e., the ratio of (output signal at opt_1 of bdc_2) : (output signal at opt_2 of bdc_2). As shown in Fig. 6, by setting the wgs_1/wgs_2 path length L to be 100.06μm/100μm with ΔL of 0.06μm, we can roughly get a 90:10 splitter by Lumerical simulation. This 90:10 splitter will be checked and verified on the fabricated devices later.

After the MZIs layout is finished with Kalyout, we use Klayout layout to run another Lumerical simulation. The simulated FSR is added as column "Klayout Simulated FSR" in Table 1. Very minor FSR difference is observed between these two simulated FSRs at lager ΔLs, and the FSR difference is around 5% at ΔL of 25μm.

The MZI transfer function and FSR will be measured on the fabricated devices to cross check with both the Lumerical simulation result and the Klayout simulation result.

TABLE I
SIMULATED AND EXPERIMENTAL FSRS AT DIFFERENT ΔL

ΔL (μm)	Lumerical Simulated FSR (nm)	Klayout Simulated FSR (nm)	Exp. FSR (nm)	ΔLxFSR (Lumer.sim.)	Exp. FSR (nm) –dup.
400	1.429	1.4272	1.425	571.44	1.435
200	2.85	2.8546	2.855	569.98	2.86
100	5.669	5.6688	5.715	566.867	5.635
50	11.345	11.2978	11.555	567.265	11.51
25	22.837	21.7167	23.37	570.933	23.31

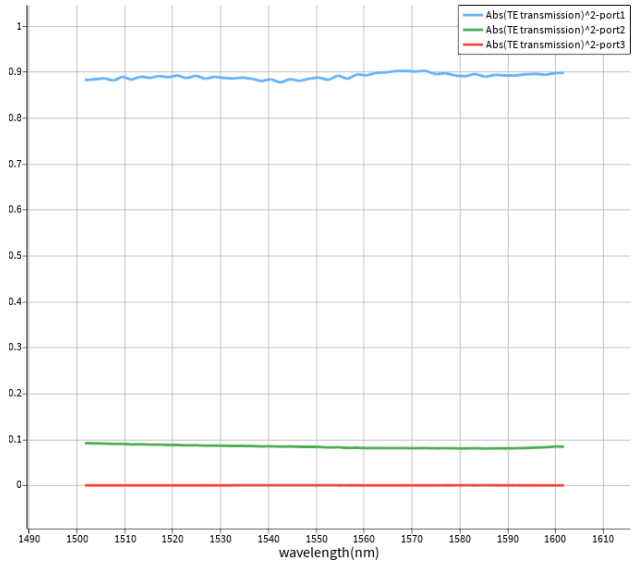

Fig. 6. Transmission amplitude at ΔL of 0.06μm.

Due to the manufacturing variation, for example, wafer to wafer, die to die, and even within die, the fabricated structural feature, say, width/height, may be slightly devout from, and vary around, the as-layout and/or the nominal width/height. Monte Carlo simulation on ΔL of 400μm is setup with parameters in Fig. 7 to simulate the manufacturing variation impact. Fig. 8 – 10 show the histogram peak gain, FSR, and wavelength, respectively. The peak gain range is -17.6049 - -5.44545dB. The FSR range is 1.42407 – 1.44654nm. The wavelength range is 1547.62 – 1549.02nm.

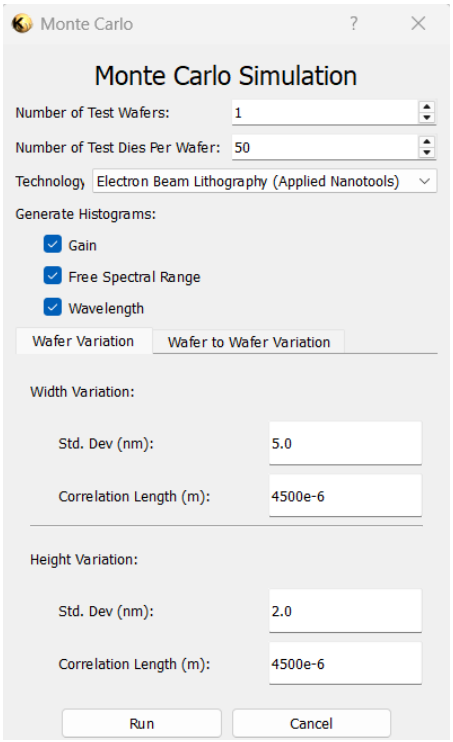

Fig. 7. Monte Carlo Simulation Setup for ΔL=400µm.

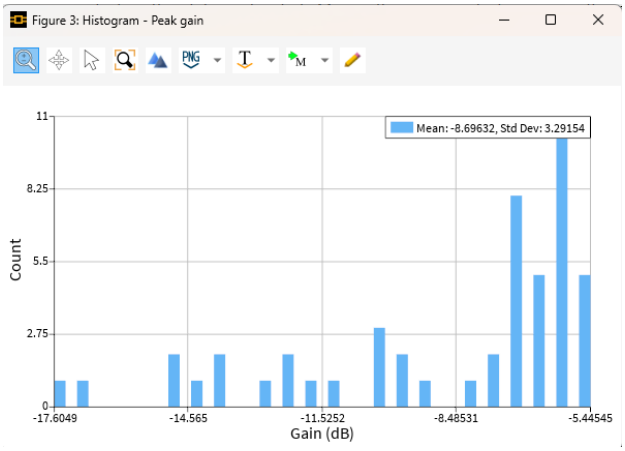

Fig. 8. Histogram peak gain from Monte Carlo simulation.

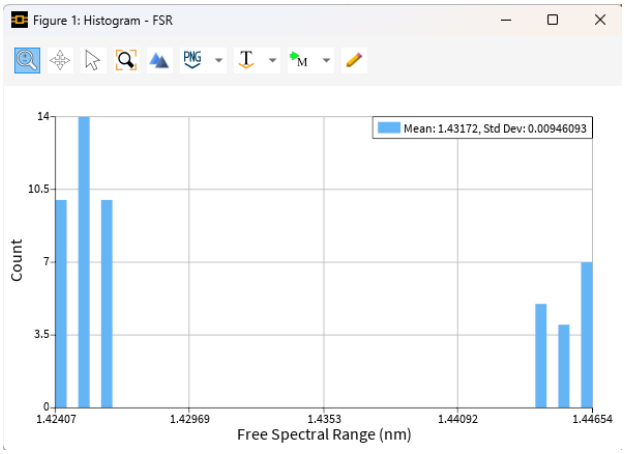

Fig. 9. Histogram FSR from Monte Carlo simulation.

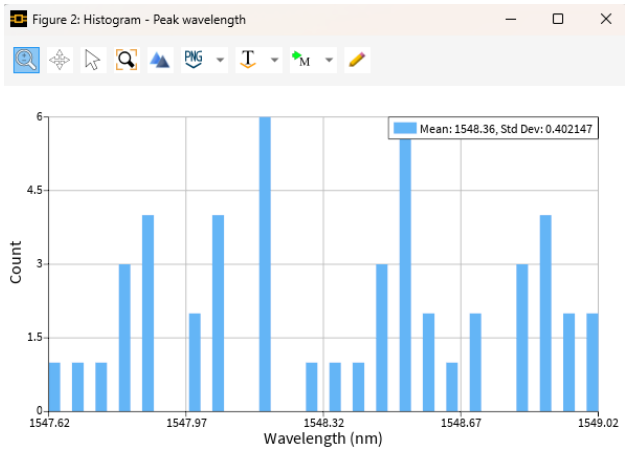

Fig. 10. Histogram wavelength from Monte Carlo simulation.

IV. Experimental Result

Different MZI transfer function plots with ΔL=400µm MZI are shown in Fig. 11, Fig. 12 and Fig. 13, with zoomed-in wavelength range of 1545nm to 1555nm to clearly show the details. Fig. 14 shows zoomed out of Fig. 13 with wavelength range of 1500nm to 1570nm. The "Lumerical Sim" ("pure" ideal no-loss Lumerical Simulated, without actual layout) plot, the "Exp_Baseline_Correction" (Experimental with baseline correction) plot, and the "Exp_Fit_w_Autocorrection" (Experimental with fit with autocorrection) plot are peaked at 0dB or around 0dB – the "Lumerical Sim" is done with ideal no-loss conditions with precise 0dB peak; the "Exp_Baseline_Correction" and "Exp_Fit_w_Autocorrection" are done with compensation to make peaks close to 0dB. The "Exp" (experimental/measured result from the manufactured structures) plot is peaked at around -22dB – -24dB because the gain profile impact from all devices (GCs, bdc's, waveguides, etc.) are included. The "Klayout Sim" (Klayout layout based Lumerical Simulation) plot is peaked at around -5dB, and its shape curve is close to the shape curve of the "Exp" – it seems that the gain profile is included in the compact model of each component. Most probably, the big peak gain difference (-22dB – -24dB vs. -5dB) between the "Exp" and the "Klayout Sim" is due to the GC gain impact. The "Klayout Sim" peaks are shifted by around 0.2nm from other four peaks. The peaks from the other four plots are pretty close to each other.

The "Exp. FSR" matches the "Lumerical Simulated FSR" and the "Klayout Simulated FSR" to better than 2% with ΔL down to 50µm. The matching at ΔL=25µm is a little bit worse due to the FSR extraction itself is not that precise at small ΔL.

FSR extracted from a duplicated set of MZIs is included in Table 1 as column "Exp. FSR (nm) – dup." as well. The FSR variation is less than 2% between the (first, main) structure and the duplicated structure which are placed around 7mm away from each other. At ΔL=400µm, the FSR variation is only 0.01nm – 1.425nm vs. 1.435nm, for the (first, main) structure and the duplicated structure, respectively.

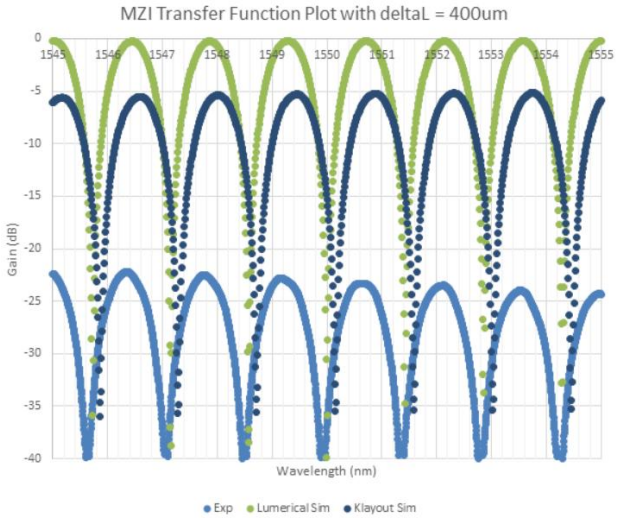

Fig. 11. Simulated and experimental MZI transfer function plots with ΔL=400µm and wavelength range of 1545nm to 1555nm

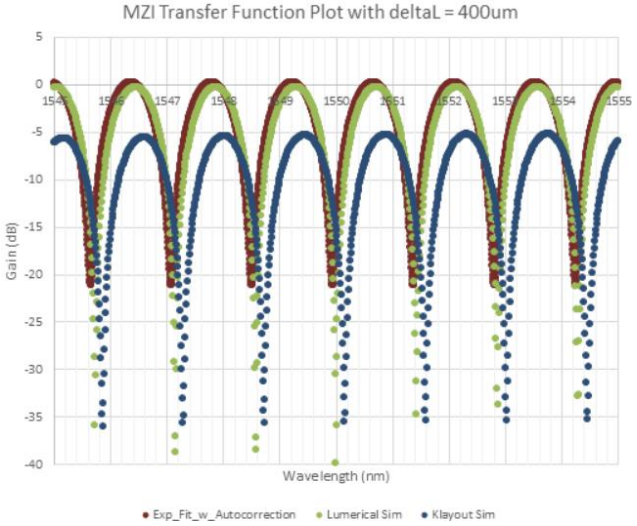

Fig. 12. Simulated and experimental-fit MZI transfer function plots with ΔL=400µm and wavelength range of 1545nm to 1555nm

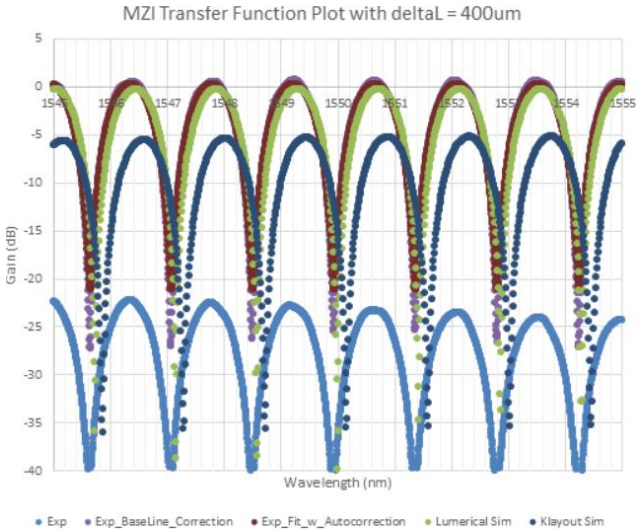

Fig. 13. Different MZI transfer function plots with ΔL=400µm and wavelength range of 1545nm to 1555nm

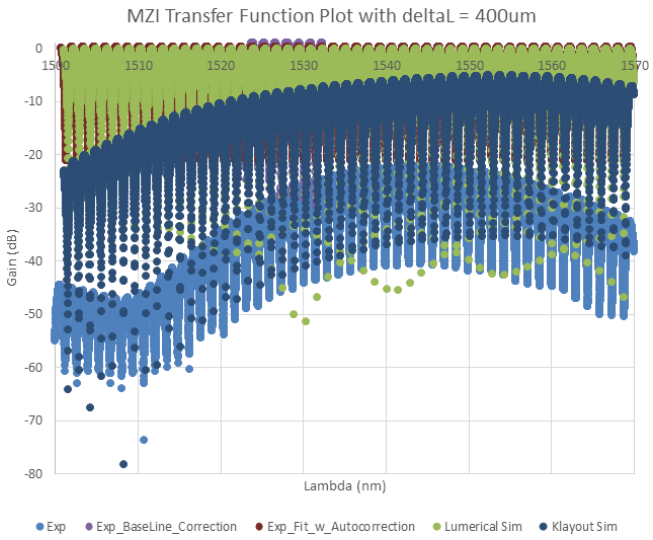

Fig. 14. Different MZI transfer function plots with ΔL=400µm and wavelength range of 1500nm to 1570nm

At ΔL=400µm, the Exp. FSR from the (first, main) structure and the duplicated structure are 1.425nm and 1.435nm, respectively – both fall inside the Monte Carlo simulated range (1.42407nm – 1.44654nm) as shown in Fig. 9.

At ΔL=400µm, the Exp. peak around 1547nm from the (first, main) structure is 1547.765nm – which falls inside the Monte Carlo simulation range (1547.62nm – 1549.02nm) as shown in Fig. 10.

At ΔL=400µm, the Exp. peak gain at around 1550nm from the (first, main) structure is around -22dB, not matching the Monte Carlo simulation range (-17.6049dB – -5.44545dB) as shown in Fig. 8. First, the above Monte Carlos simulation does not cover the GC gain impact. Second, as we may know, the relative GC location in the vertical direction may greatly impact the measured/ experimental peak gain. We will see the GC location impact when we analyze the insertion loss later.

The waveguide parameters (n_1, n_2, n_3) extracted from the (first, main) ΔL=400µm structure experimental result are n_1 = 2.4234, n_2 = -1.1473, n_3 = -0.0261, and n_{g0} = 4.1845.

At ΔL=400µm, the group index (n_g) extracted from the experimental result from the (first, main) structure and from the nominal (w/h of 500nm/220nm) eigenmode Lumerical simulation are plotted in Fig. 15. The extracted group index (n_g) is not matching to, and is shifted up from, the nominal eigenmode Lumerical simulation – indicating the waveguide width/height may not be at the exact nominal values – in other words, manufacturing variation may play into the role and bring non-nominal values.

Based on historical data from multiple similar runs, the typical waveguide width (w) variation is between 470nm and 510nm, and the typical waveguide height (h, which is also the thickness) variation is between 215.3nm and 223.1nm. The four corner conditions are w/h = 470nm/215.3nm, 470nm/223.1nm, 510nm/215.3nm, and 510nm/223.1nm. With ΔL=400µm, the group index (n_g) extracted from the experimental result from the (first, main) structure and from the nominal and four corner conditions (five in total)

eigenmode simulations are plotted in Fig. 16. The group index (n_g) extracted from the experimental result falls within the span defined by the four corner conditions – indicating the actual device width/height falls within the four corner conditions. The group index (n_g) at 1550nm is 4.1857.

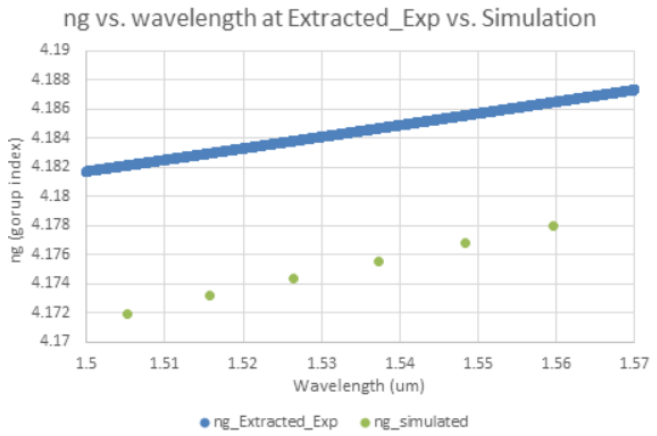

Fig. 15. Group index (n_g) extracted from experimental result and from nominal eigenmode Lumerical simulation for the (first, main) structure with ΔL=400μm

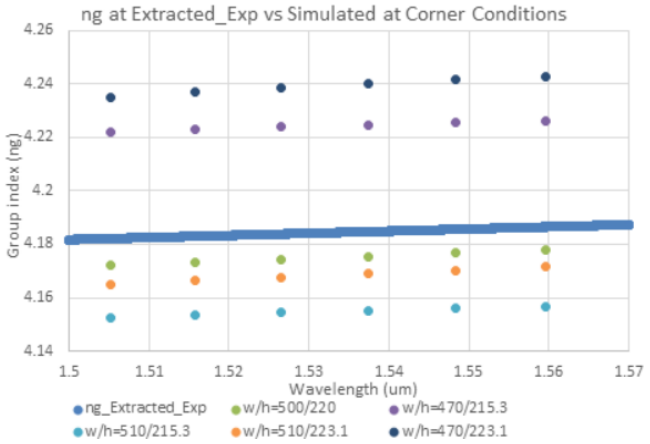

Fig. 16. Group index (n_g) extracted from experimental result and from eigenmode Lumerical simulations with nominal and four corner conditions for the (first, main) structure with ΔL=400μm

Is there any way to find/extract the unique effective (device) width/height? Yes, theoretically it is doable. Each waveguide width/height combination has a unique set of eigenmode waveguide parameters (n_1, n_2, n_3), and each set of eigenmode waveguide parameters (n_1, n_2, n_3) has a unique (group index (n_g) vs. wavelength) relation. Thus there is a unique relation between the (group index (n_g) vs. wavelength) relation and the width/height combination. One may find the unique effective (device) width/height based on the (group index (n_g) vs. wavelength) relation (or the set of waveguide parameters (n_1, n_2, n_3)). Practically, it may not make that much sense because the effective width/height varies not only with manufacturing process run, but also with the relation location even within the same die/wafer – in other words, the effective width/height is very local – it is device dependent and location dependent. For example, at ΔL=400μm, we see 0.01nm FSR variation (l.425 vs. 1.435nm) between the (first, main) MZI and the duplicated MZI which are placed around 7mm away from each other. The corresponding width/height variation will be evaluated later.

Fig. 17 shows the simulated group index (n_g) with more w/h conditions for the (first, main) structure with ΔL=400μm. The simulation result with w/h of 501nm/221nm matches the extracted group index (n_g) very well, while the simulation results with w/h of 498nm/221nm / 504nm/221nm, are slightly shifted above / below the extracted group index (n_g), respectively, strongly verifying that w/h of 501nm/221nm is a reasonable extraction for this device.

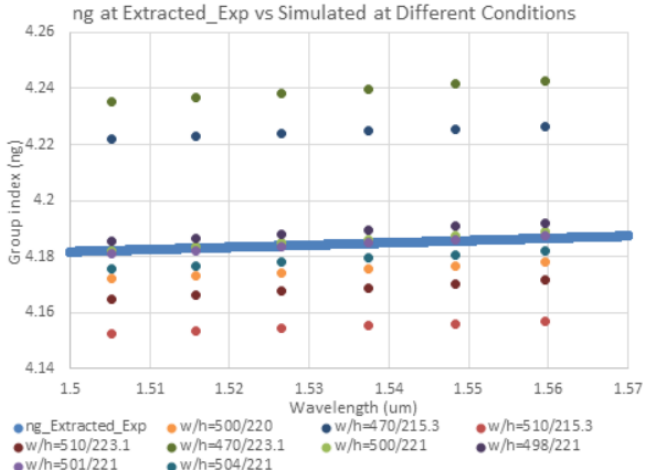

Fig. 17. Group index (n_g) extracted from experimental result and from eigenmode Lumerical simulations with different width/height conditions for the (first, main) structure with ΔL=400μm

Fig. 18 shows the simulated group index (n_g) with more w/h conditions for the duplicated structure with ΔL=400μm. The simulation result with w/h of 503nm/220.5nm matches the extracted group index (n_g) very well. The group index (n_g) at 1550nm is 4.1823.

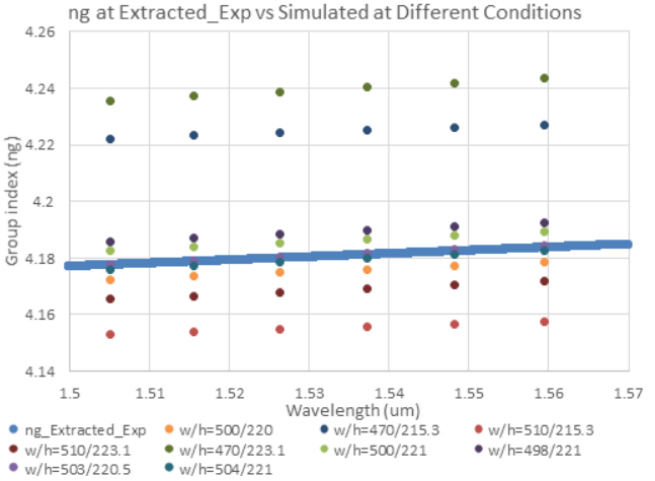

Fig. 18. Group index (n_g) extracted from experimental result and from eigenmode Lumerical simulations with different width/height conditions for the duplicated structure with ΔL=400μm

The duplicated ΔL=400μm structure is placed around 7mm from the (first, main) structure in the layout. The around 7mm separation causes a width shift of 2nm (501 vs. 503nm), a height shift of 0.5nm (221 vs. 220.5nm), a FSR shift of 0.01nm (1.425 vs. 1.435nm), and a group index (n_g) shift of 0.0034 (4.1857 vs. 4.1823). All the difference is within 1%.

The above comparison shows structural feature w/h is pretty local, and may be good for local usage only. The local w/h may not be used for other devices nor be used as a universal value for all devices across the wafer.

The 5-order polynomial smoothened experimental output plot for the (first, main) 90:10 splitter (100.06μm/100μm) is shown in Fig. 19. The amplitude peak is at 1543.015nm. The peak amplitude ratio of (channel_1/channel_2) is 2.23, which corresponds to a 69:31 split, rather than the expected 90:10 split. The actual effective ΔL extracted from Eq. 1 is 121.39nm, which is 61.39nm longer than the designed 60nm. From the duplicated 90:10 splitter, which is around 7mm away from the (first, main) 90:10 splitter, the amplitude peak is at 1552.435nm; the peak amplitude ratio is 3.37, corresponding to a 77:23 split; the actual effective ΔL extracted from Eq. 1 is 102.82nm, which is 42.82nm longer than the designed 60nm.

The 5-order polynomial smoothened experimental output plot for a balanced 200μm/200μm MZI is shown in Fig. 20. The amplitude peak is at 1552.565nm, and the peak amplitude ratio of (channel_1/channel_2) is 22.14, which corresponds to a 96:4 split. The actual effective ΔL extracted from Eq. 1 is 41.39nm, rather than the balanced 0 as expected.

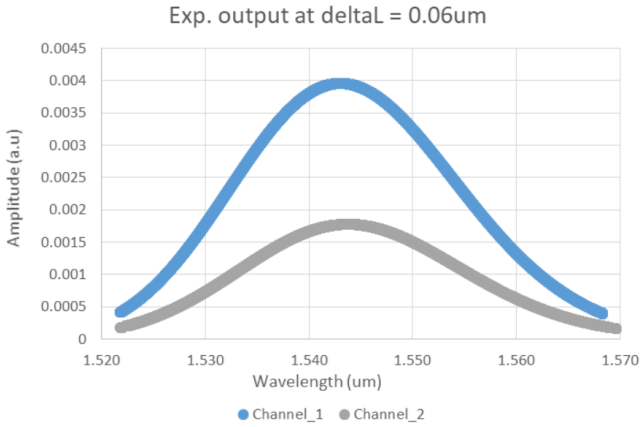

Fig. 19. Output from a 90:10 splitter (100.06μm/100μm).

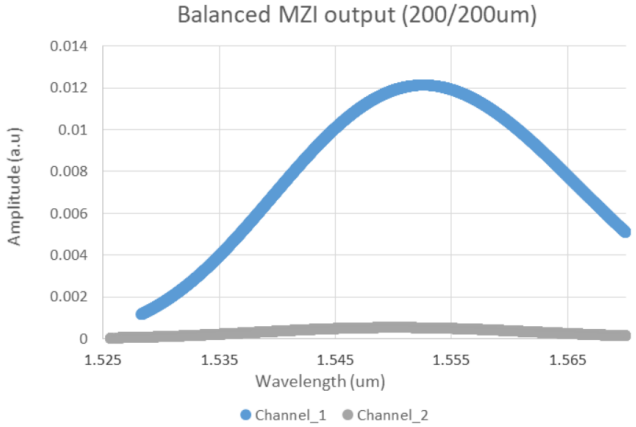

Fig. 20. Output from a balanced MZI (200μm/200μm).

In short, conceptually, the manufacturing variation may introduce an "effective" extra path length difference into the MZIs. The "effective" extra path length difference may vary from device to device, and from location to location.

Two de-embedding structures with waveguide length of 250μm and 500μm are used to calibrate the measurement system insertion loss, and to measure the silicon waveguide intrinsic loss if possible. The 5-order polynomial smoothened experimental insertion loss plots from the (first, main) structures and the duplicated structures (which are placed around 7mm away from the (first, main) structures) are shown in Fig. 21. The measurement system insertion loss is around 23dB with 1543.17nm peak wavelength for the (first, main) structures and around 18dB with 1553.01nm peak wavelength for the duplicated structures. The measurement system insertion loss is around 5dB less for the duplicated structures. One possible reason is the laser and/or detectors are placed relatively closer to the duplicated structures than the (first, main) structures and stronger light signal is collected during the measurements. As shown in zoomed-in Fig. 22 and Fig. 23, the peak insertion loss is 22.66dB at 1543.17nm (L=250μm), 22.80dB at 1543.885nm (L=500μm), 18.11dB at 1553.01nm (L=250μm_dup), and 18.36dB at 1553.395nm (L=500μm_dup), respectively. The longer length de-embedding structures show longer peak wavelength than the shorter length de-embedding structures.

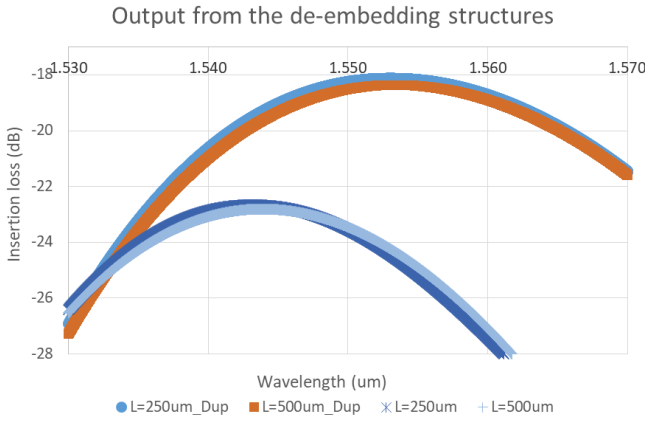

Fig. 21. Insertion loss output from 2 sets of de-embedding structures with two waveguide lengths

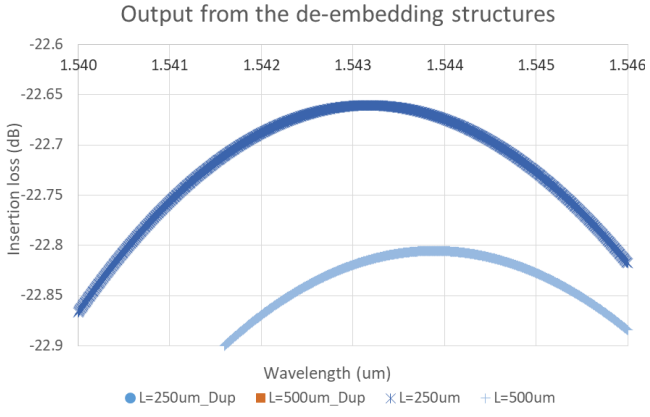

Fig. 22. Zoomed-in of Fig. 21 around the (first, main) structure peaks

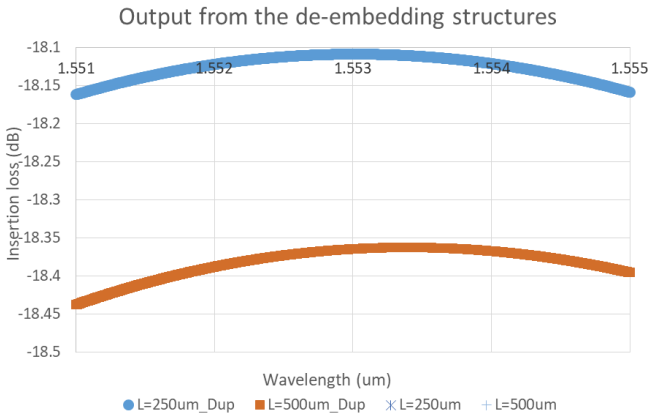

Fig. 23. Zoomed-in of Fig. 21 around the duplicated structure peaks

The 5-order polynomial smoothened experimental insertion loss plots from another set of de-embedding structures with three lengths 140µm, 420µm and 1188.8µm are shown in Fig. 24. As shown in zoomed-in Fig. 25, the peak insertion loss is 17.46dB at 1551.155nm (L=140µm), 17.73dB at 1551.755nm (L=420µm), and 18.38dB at 1552.18nm (L=1188.8µm), respectively. Again, the longer length de-embedding structures show longer peak wavelength than the shorter length de-embedding structures.

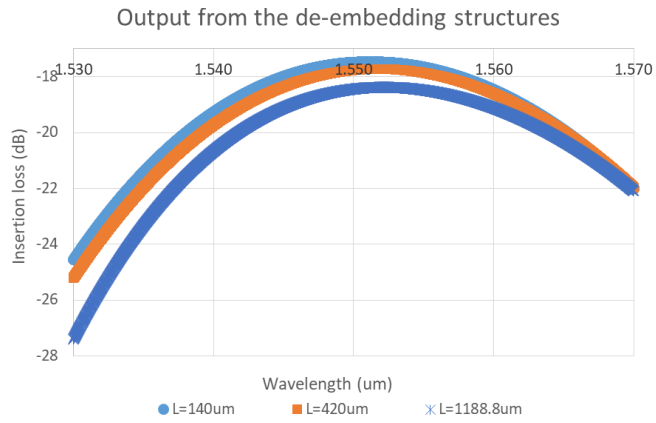

Fig. 24. Insertion loss output from de-embedding structures with three waveguide lengths

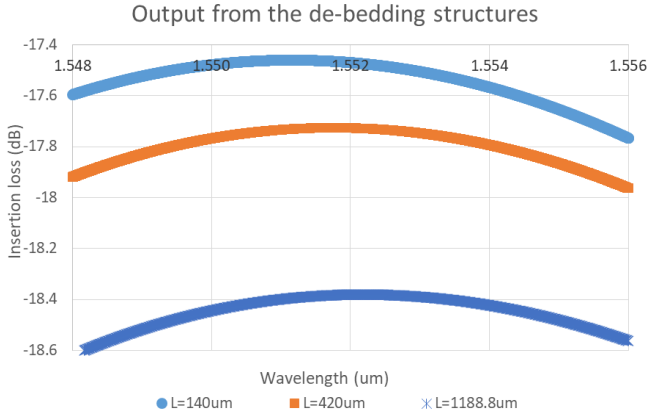

Fig. 25. Zoomed-in of Fig. 24 around the peaks

What are the possible reasons for the longer length de-embedding structures showing longer peak wavelength than the shorter length de-embedding structures?

Typically, lasers can exhibit a red shift in the peak wavelength due to temperature changes. This shift occurs because temperature affects the material properties of the laser medium, causing a change in its refractive index and physical dimensions, both of which influence the laser's peak wavelength. Specifically, as temperature increases, the peak wavelength of the emitted light generally increases – so-called red shift [7].

In the layout, the shorter length de-embedding structures are placed towards the left side, while the longer length de-embedding structures are placed towards the right side, of the 605µm x 410µm basic block. The date/time stamps from the experimental result files show the longer length de-embedding structures are tested shortly (within a few minutes) after the shorter length de-embedding structures. One possible reason may be the laser intrinsic peak wavelength variation itself. Another possible reason may be a guess that the laser temperature may slightly increase when moving from the shorter length de-embedding structures to the longer length de-embedding structures due to the accumulated usage, and the slight laser temperature increase causes the red-shift, i.e., peak wavelength increase, in laser output. To check and verify these two possible reasons, measurement on the same de-embedding structure may be repeated continuously for multiple, say, 20, times. If the peak wavelength is pretty random with measurement times, then the laser intrinsic peak wavelength variation itself may be the reason. If the peak wavelength keeps red shifting with measurement times, then the laser temperature increase due to accumulated usage may be the reason. To further verify this, some mechanism to track the laser internal temperature may need to be added and tracked.

For the de-embedding structures, the measurement system insertion loss is from two parts: the insertion loss from the two "pure" grating couplers (GCs) without counting any length of waveguide, and the intrinsic loss from the entire routing waveguide which is proportional to the waveguide length. The insertion loss from the two "pure" GCs may vary depending on how close the laser and/or detectors are aligned to the two GCs, especially in the vertical direction – the closer, the smaller insertion loss is.

Fig. 26 shows the measurement system insertion loss vs. waveguide length (in cm) plots for three sets of de-embedding structures. Within each set of de-embedding structures, the de-embedding structures are placed around 100 - 500µm from each other. With the first order approximation, it may be reasonable to assume the laser and/or detectors alignment to the GCs in de-embedding structures is the same for all de-embedding structures within the same set. In this way, one may decouple the measurement system insertion loss and use linear fitting to extract the insertion loss from the two "pure" GCs (which is a constant and independent of the waveguide length) and the intrinsic waveguide loss (which is proportional

to the waveguide length). As shown in Fig. 26, with the three-length set, the fitting R^2 is 0.9992, verifying it is a good fit. The extracted insertion loss from the two "pure" GCs is 22.52dB, 17.86dB, and 17.35dB, respectively. The extracted waveguide intrinsic loss is 5.6dB/cm, 10dB/cm, and 8.7dB/cm, respectively. The average waveguide intrinsic loss is 8.1dB/cm, and the standard deviation is 1.8dB/cm. The waveguide intrinsic loss is 8.1±1.8dB/cm at 1550nm TE. The insertion loss from the two "pure" GCs variation is 5.17dB among the three sets, which is equivalent to the intrinsic loss from a 6.38mm long waveguide. This indicates the close and stable laser and/or detectors alignment to the GCs, mainly in the vertical direction, is very critical to minimize and/or stabilize the measurement system insertion loss.

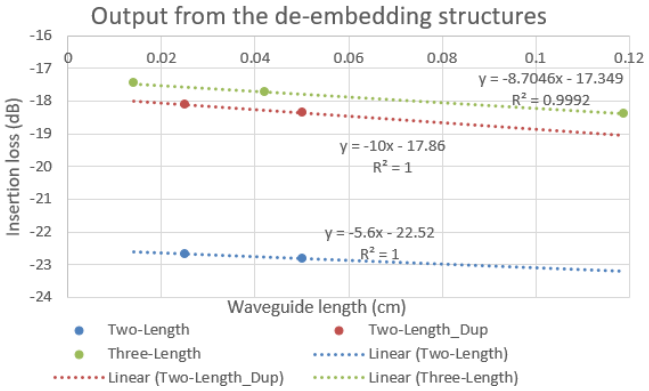

Fig. 26. Insertion loss vs. waveguide length (cm) for 3 sets of de-embedding structures

Compared to the around 1 - 2dB/cm waveguide intrinsic loss reported in [8] [9], the extracted 8.1dB/cm at 1550nm TE is around 4-8x higher. Also, compared to the average intrinsic loss 8.1dB/cm, the standard deviation 1.8dB/cm is significant. It sounds like the first order approximation used in the above analysis may not be that solid. To minimize the cross impact from the insertion loss from the two "pure" GCs variation, better control on the laser and/or detectors alignment to the two GCs, especially in the vertical direction, may be needed. In each set, only two or three different waveguide lengths on the order of 100µm are used. Multiple, say 10 if possible, different waveguide lengths, especially some at longer wavelength on the order of cm, may be needed to minimize the measurement errors. Better average intrinsic loss and better standard deviation are expected with the above two improvements.

V. Conclusion

On FSR, the experimental results match the simulations to better than 2% at path length difference down to 50µm. The matching at path length difference of 25µm is a little bit worse due to the FSR extraction itself is not that precise at small path length difference. At 400µm path length difference, both the experimental FSR and the experimental peak wavelength fall within the Monte Carlo simulation range, while the experimental peak gain does not fall within the Monte Carlo simulation range because the grating coupler (GC) impact is not included in the Monte Carlo simulation. The group index extracted from the experimental result falls within the span defined by the four corner conditions. Local effective device width/height may be extracted from the group index matching between experimental and eigenmode simulation. A 0.01nm FSR difference (1.425 vs. 1.435nm), a 0.0034 group index difference (4.1857 vs. 4.1823), a 2nm width difference (501 vs. 503nm), and a 0.5nm height difference (221 vs. 220.5nm), are observed when two MZIs with 400µm path length difference are placed around 7mm away. Due to the manufacturing variation, structural feature w/h is pretty local, and may be good for local usage only. The local w/h may not be used for other devices nor be used as a universal value for all devices across the wafer. Two designed 90:10 splitters, which are placed around 7mm away, become one 69:31 splitter and one 77:23 splitter due to the conceptual introduction of an "effective" extra path length difference of 61.39nm and 42.82nm, respectively, induced by the manufacturing variation. Similarly, the designed balanced MZI becomes a 96:4 splitter with an introduced "effective" extra path length difference of 41.39nm. The manufacturing variation induced "effective" extra path length difference may vary from device to device, and from location to location. The extracted waveguide intrinsic loss is 8.1±1.8dB/cm at 1550nm TE. Better average intrinsic loss and better standard deviation may be expected with design and measurement improvements. The close and stable laser and/or detectors alignment to the GCs, especially in the vertical direction, is very critical to minimize and/or stabilize the measurement system insertion loss.

References

[1] N. Saha, G. Brunetti, A. Toma, M. Armenise, and C. Ciminelli "Silicon Photonic Filters: A Pathway from Basics to Applications," *Adv. Photonics Res. 2024, 5, 2300343*, pp. 1–44.

[2] https://www.electronicdesign.com/technologies/embedded/article/55278472/openlight-silicon-photonics-transforms-data-centers-and-ai-advancement

[3] R. S. Shamy, A. E. Afifi, M. M. Badr, and M. A. Swillam, "Modelling, characterization, and applications of silicon on insulator loop terminated asymmetric Mach Zehnder interferometer," *Scientific Reports volume 12, Article number: 3598 (2022)*.

[4] A. M. Taha; S. Yousuf; M. S. Dahlem and J. Viegas, "Highly-Sensitive Unbalanced MZI Gas Sensor Assisted With a Temperature-Reference Ring Resonator", IEEE Photonics Journal, VOL. 14, NO. 6, 6657709.

[5] L. Vivien, F. Grillot, E. Cassan, D. Pascal, S. Lardenois, A. Lupu, S. Laval, M. Heitzmann, and J.-M. Fédéli, "Comparison between strip and rib SOI microwaveguides for intra-chip light distribution", Optical Materials, Volume 27, Issue 5, February 2005, Pages 756-762

[6] https://www.mathsisfun.com/geometry/symmetry-point.html

[7] https://www.arroyoinstruments.com/blog/how-does-temperature-affect-the-wavelengths-of-lasers/?srsltid=AfmBOoqRC2p-DZMHJzVlNDOn9HodtooH8I2lfrSkFs0deUomUw7zxVeH

[8] W. Bogaerts and L. Chrostowski, "Silicon Photonics Circuit Design: Methods, Tools and Challenges", *Laser Photonics Rev. 2018, 1700237*

[9] https://siepic.ca/openEBL/